

<https://doi.org/10.1038/s41612-026-01358-z>

Remote modulation of European blocking on 2022 Pakistan summer extreme rainfall: the bridge role of Tibetan Plateau

Check for updates

Jiaxin Ye^{1,2}, Xingwen Jiang^{1,2}✉, Tuantuan Zhang³, Chao Chen^{1,2} & Huimei Wang^{1,2}

In the summer of 2022, extreme rainfall struck Southern Pakistan, causing catastrophic floods and severe damage to both ecosystems and human communities. Previous studies have linked this extreme rainfall to the European blocking high, yet the underlying physical pathways remain elusive. Using observational data and numerical simulation, this study demonstrates a critical bridge role of the Tibetan Plateau (TP) in conveying the remote effects of European blocking on Pakistan rainfall. On the one hand, the extreme rainfall deficiency around the southeastern TP and its attendant anomalous diabatic cooling directly drive pronounced lower-level easterly anomalies over the northwestern Indian subcontinent, thereby channeling moisture westward and boosting rainfall within Southern Pakistan. This mechanism surpasses the influence of moderate tropical SST anomalies observed in this year. On the other hand, the southeastern TP rainfall itself is regulated by the record-breaking European blocking. The enhanced European blocking stimulates an atmospheric Rossby wave train propagating to the east of the TP and reinforces the anomalous upper-tropospheric anticyclone there. This anticyclone, combined with unique thermal structure over the TP, induces intense descent and reduced rainfall around the southeastern TP. Both statistical analysis during 1979–2022 and model simulation results jointly corroborate these physical processes observed in 2022. Hence, this study clearly establishes the physical linkage among European blocking, TP heating, and Pakistan extreme rainfall.

Pakistan lies in the semi-arid to arid belt of western South Asia^{1,2}. The summer monsoon supplies 65–75% of the total annual rainfall in Pakistan, which is of great importance for both natural ecosystems and socio-economic development there^{3,4}. However, dramatic fluctuations in monsoon rainfall frequently result in catastrophic floods. In the summer of 2022, unprecedented extreme rainfall hit Pakistan, particularly the accumulated rainfall amount in August notably surpassing 500% of its climatological mean^{5,6}. During this event, record-breaking rainfall anomalies swept across a large area of southern Pakistan, including southern Baluchistan and Sindh (Fig. 1a). This catastrophic event broke the rainfall record set in 2010, internally displacing about 32 million people, causing 1486 fatalities, with the economic losses up to \$30 billion^{7,8}. Therefore, understanding the drivers of this devastating rainfall in Pakistan remains an important question to be addressed, essential for improving the accuracy of extreme precipitation prediction.

It is widely accepted that tropical air-sea interactions, such as El Niño-Southern Oscillation (ENSO) and Indian Ocean dipole (IOD), shape the South Asian summer monsoon (SASM) rainfall by modulating the Walker circulation and local Hadley circulation^{9–12}. When La Niña occurs, ascending limb of Walker circulation over the Indian sector strengthens, favoring enhanced rainfall over the South Asian monsoon region, whereas El Niño causes drought^{13,14}. Hong et al. (2023) proposed that the observed La Niña in the summer of 2022 could induce anomalous easterly moisture transport and contribute to this extreme Pakistan rainfall¹⁵. However, most areas of Pakistan belong to the edge of the South Asian monsoon region. The Pakistan rainfall-ENSO relationship is weaker than the SASM-ENSO relationship, which is supported by both the observations and numerical experiments¹⁶. Moreover, La Niña alone cannot explain such catastrophic 2022 Pakistan floods due to its moderate amplitude in this year^{15,16}. In terms of the IOD signal, its linkage with Pakistan rainfall is also tenuous, with their

¹Heavy Rain and Drought-Flood Disasters in Plateau and Basin Key Laboratory of Sichuan Province, Institute of Tibetan Plateau Meteorology, China Meteorological Administration, Chengdu, China. ²Institute of Tibetan Plateau Meteorology, Chinese Academy of Meteorological Sciences, Beijing, China. ³School of Atmospheric Sciences, Sun Yat-sen University; and Southern Marine Science and Engineering Guangdong Laboratory (Zhuhai), Zhuhai, China.

✉ e-mail: jiangxingwen@cma.gov.cn

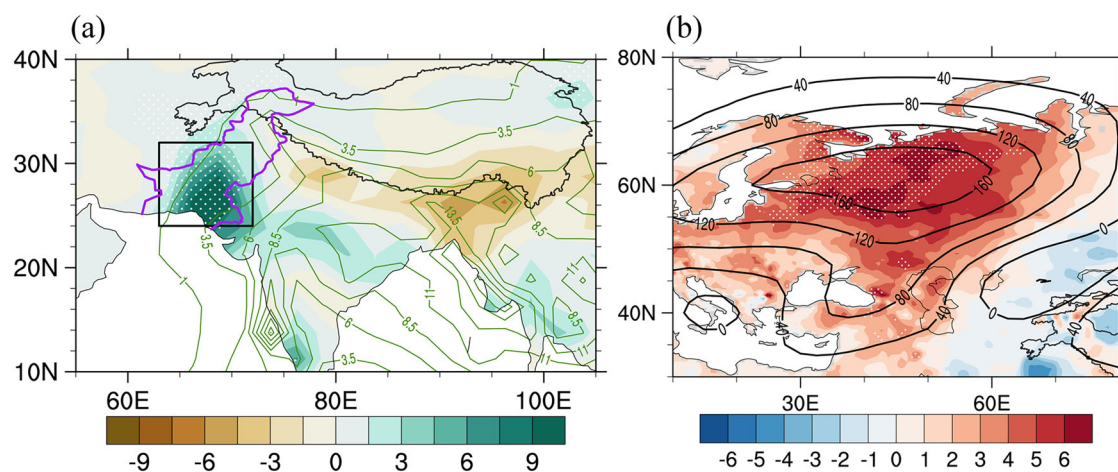


Fig. 1 | The observed precipitation and maximum surface air temperature anomaly in August 2022. a The precipitation anomaly in 2022 (mm day^{-1} ; shading) and precipitation in climatology (mm day^{-1} ; contour). The box outlines the region ($64^{\circ}\text{--}72^{\circ}\text{E}/24^{\circ}\text{--}32^{\circ}\text{N}$) for defining the Southern Pakistan rainfall index (SPRI),

while the purple outline represents the border of Pakistan. **b** The maximum surface air temperature anomaly ($^{\circ}\text{C}$; shading) and geopotential height anomaly at 200 hPa (gpm; contour). The white dot in (a, b) indicates the largest rainfall/surface air temperature anomaly since 1979.

correlation coefficient less than 0.1 during 1958–2010¹⁷. Collectively, these studies imply that the individual tropical sea surface temperature (SST) is insufficient in explaining the variability of Pakistan precipitation.

Beyond the tropical sea-atmosphere interaction, mid- and high-latitude processes also have potential impacts on Pakistan precipitation. Concurrent with the extreme Pakistan rainfall in August 2022, a severe heatwave swept across Northwestern Russia, coinciding with an exceptionally strong European blocking high (Fig. 1b)¹⁵. Similar Russian heatwave-Pakistan flooding configuration also occurred in the summer of 2010, and numerous studies attributed it to a large-scale atmospheric Rossby wave train that emanated from the enhanced European blocking high, crossed the vicinity of Lake Baikal, and reached the north China-Tibetan Plateau region^{18–21}. Downstream energy dispersion from the European blocking region deepened the trough northwest of Pakistan, triggering anomalous ascending motions and heavy rainfall over northern Pakistan in late July and early August of 2010^{18,20,22}. In the summer of 2022, Hong et al. (2023) and Hu et al. (2024) likewise suggested a potential influence of European blocking on Pakistan precipitation through the physical pathway akin to that documented for the 2010 event^{15,23}. Beyond inducing anomalous ascent, whether and how mid-high latitude atmospheric circulations modulate the anomalous moisture transport into Pakistan remain unrevealed. Meanwhile, the extreme rainfall in 2022 mainly confined to southern Pakistan⁶, hinting that the direct influence of European blocking on the core precipitation region might be weaker than that in 2010.

Geographically, Pakistan lies to the southwest of the Tibetan Plateau (TP). As the highest plateau in the world situated in the subtropics of the Eurasian continent, the TP exerts significant impacts on regional and global climate due to its unique geographical position, altitude, area, and steep slopes in the south and east^{24–28}. On the one hand, the TP and its adjacent regions serve as a huge atmospheric heat source during summer, exerting profound influences on Asian summer monsoon variability^{27,29–32}. Particularly, condensational heating around the eastern TP is identified as a critical driver of Pakistan rainfall¹. On the other hand, TP thermal heating itself is also partly regulated by the mid-latitude westerly systems and SST anomalies over the North Atlantic Ocean^{33,34}. Therefore, the TP could act as a bridge that conveys the mid- and high-latitude forcing into the Asian monsoon region^{28,34}. However, the role of TP in the Pakistan extreme rainfall during the summer of 2022 is still unclear.

In this study, we first attempt to address the possible intermediate role of the TP in linking European blocking to the Pakistan extreme rainfall, based on the observational precipitation and atmospheric reanalysis data. Then, numerical simulations are also conducted with a linear baroclinic model (LBM) to vindicate the underlying physical mechanisms.

Results

The water vapor budget over Southern Pakistan and associated anomalous atmospheric circulations in August 2022

Climatologically, a prevailing south-westerly monsoon in August sweeps from the Arabian Sea across most area of the Indian subcontinent (Fig. 2a), promoting warm and moist air transport from ocean toward South Asia and bringing abundant monsoon rainfall here (Fig. 2b). Pakistan abuts the western TP and consists of plains in the southeast and the mountainous areas in the northwest (Fig. 2a). This region lies on the northwestern margin of the South Asian monsoon domain, which experiences a greatly attenuated direct influence of the south-westerlies with column-integrated moisture fluxes are substantially weaker than those over southern India (Fig. 2b). Consequently, Pakistan receives much less rainfall than areas farther south, with the climatological mean rainfall in August gradually decreasing from $\sim 4 \text{ mm day}^{-1}$ in south-eastern Pakistan to $< 1 \text{ mm day}^{-1}$ in the northwest (Fig. 2b).

In August 2022, this canonical pattern is reversed. A pronounced anomalous easterly flow exceeding -3 m s^{-1} at lower-level replaces the climatological mild westerly flow over the northwestern Indian subcontinent (Fig. 2a, c). Guided by this reversed flow, abnormal water vapor originating from Bangladesh and Bay of Bengal migrate zonally along the Himalayan foothills with the maximum flux magnitudes exceeding $260 \text{ kg m}^{-1} \text{ s}^{-1}$, and surge into southern Pakistan, where anomalous moisture convergence reached $-2 \times 10^{-4} \text{ kg m}^{-2} \text{ s}^{-1}$ (Fig. 2d). The water vapor budget for the target region also suggests that the anomalous column-integrated water vapor fluxes at all four boundaries are opposite to their climatological states (Fig. 2b, d). Climatologically, water vapor flows into southern Pakistan through the western and southern boundaries and flows downstream mainly through the eastern boundary (Fig. 2b), while in August 2022, the flux at eastern boundary substantially switches from an export of -431.4 kg s^{-1} to an import of 156.6 kg s^{-1} (Fig. 2d). This 588.0 kg s^{-1} increase in water vapor fluxes through the eastern boundary dominates the moisture surplus in 2022 relative to the climatology (Fig. 2d), and thus fuels the rainfall intensification over the target region (Fig. 1a). These results also corroborate the moisture equation diagnosis of Luo et al. (2023), who identified the dynamic component, namely the humidity advection induced by the anomalous easterly flows, as the primary contributor to this Pakistan extreme rainfall⁶. Additionally, Hong et al. (2023) reported contributions from both westward moisture transport from the Bay of Bengal and eastward moisture transport from the Arabian Sea to Pakistan extreme rainfall in summer 2022, with the former far exceeding the latter¹⁵. It is worth noting that Hong et al. (2023) examined the July–August mean state¹⁵, whereas our analysis focuses on the condition in August. Despite this difference, their

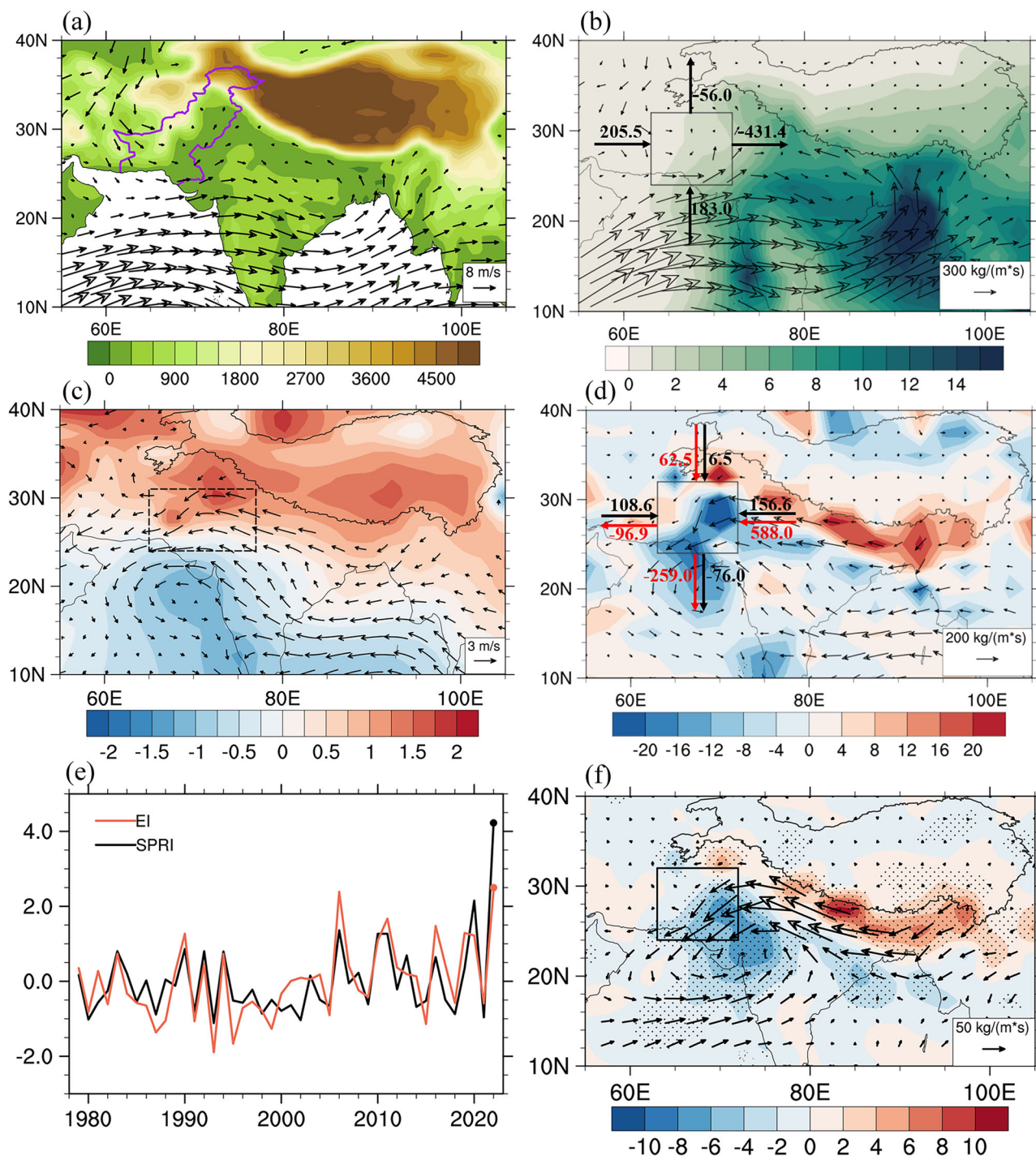


Fig. 2 | The moisture transport and associated lower-level atmospheric circulations in August. a The topographic height (m; shading) and horizontal wind at 850 hPa of climatology (m s^{-1} ; vector). **b** The column-integrated moisture flux (from surface to 300 hPa; $\text{kg m}^{-1} \text{s}^{-1}$; vector) and precipitation (mm day^{-1} ; shading) of climatology. The numbers denote net water vapor input (positive) or output (negative) (Kg s^{-1}) across four boundaries of the key region. **c** The anomalies of horizontal wind at 850 hPa (m s^{-1} ; vector) and surface pressure (hPa; shading) in

2022, with the dashed box outlines the region for defining the easterly index (EI). **d** The anomalies of column-integrated moisture flux ($\text{kg m}^{-1} \text{s}^{-1}$; vector) and its divergence ($\times 10^{-5} \text{kg m}^{-2} \text{s}^{-1}$; shading) in 2022. The black and red numbers/thick arrow denote net water vapor input (or output) in 2022 and their departure from the climatology, respectively. **e** The standardized time series of SPRI (black) and EI (red) from 1979 to 2022. **f** Same as in (d), but for the regressions against the standardized EI during 1979–2022, in which black dots denote significance at $p = 0.05$ level.

findings generally align with our conclusion that the westward moisture transport originating around the Bay of Bengal dominates the moisture supplement within southern Pakistan.

Given the role of the anomalous lower-tropospheric easterlies over the northwest Indian subcontinent in triggering Pakistan extreme rainfall in August 2022, we define an easterly index (called the EI) to depict the features

of this easterly flow (Fig. 2e). The EI is calculated as the August mean zonal wind anomalies at 850 hPa averaged over 65°E – $77^{\circ}\text{E}/24^{\circ}\text{N}$ – 31°N (denoted by the rectangle in Fig. 2c) and multiplied by -1 to be consistent with the situation in 2022, that is, positive values denote strengthened easterlies. Figure 2f shows the regression map of August mean moisture transport relative to the EI during 1979–2022. As the anomalous easterly wind

accelerated, a pronounced westward moisture corridor along the southern flank of the Himalayas and moisture convergence over southern Pakistan tend to be strengthened (Fig. 2f), which contributes to enhanced precipitation here. These regressed patterns align closely with the observations in 2022 (Fig. 2d, f). Accordingly, EI shows a significant correlation coefficient up to 0.78 with the Southern Pakistan rainfall index (SPRI; defined in Fig. 1a) during 1979–2022, explaining approximately 60.8% of SPRI variance (Fig. 2e). At the same time, the EI in 2022 reaches 2.3 m s^{-1} , about 2.4 standard deviations above the 1979–2022 mean and the highest value since 1979, corresponding to the record-breaking SPRI (Fig. 2e), which could well explain the extremity of precipitation in southern Pakistan. It is noteworthy that the EI in 2006 is comparable to that in 2022, ranking as the second strongest after 2022 (Fig. 2e). In August 2006, pronounced westerly moisture transport appears from the tropical Arabian Sea to Indian Peninsula (Supplementary Fig. 1a), whereas such transport is invisible in 2022. The strong eastward moisture transport conflicts with westward moisture transport along the Himalayas, causing intense moisture convergence over the central Indian Peninsula (Supplementary Fig. 1a), with the anomalous precipitation center mainly appearing in the regions to the southeast of Pakistan (Supplementary Fig. 1b). Therefore, the SPRI in 2006 exhibits a weaker positive anomaly than that in 2022 (Fig. 2e). Although moisture transport from the tropical Arabian Sea plays a relatively minor role in this 2022 extreme event, it may also exert a certain modulation on Pakistan rainfall variability from a long-term perspective¹⁵.

The above results imply that the anomalous lower-level easterly flow over the northwest Indian subcontinent is pivotal to the Pakistan extreme rainfall in August 2022 by channeling excessive moisture into southern Pakistan. We therefore investigate the possible mechanisms of the anomalous easterly flow in the following section.

Direct impact of TP thermal forcing on the anomalous lower-level easterly flow over the northwestern Indian subcontinent

As reviewed in the introduction, the variability of the SASM has been traditionally linked to the remote forcing of slow-varying SST anomalies, especially the tropical Indo-Pacific Ocean. In August 2022, the tropical SST anomalies exhibit a central Pacific type of La Niña and a negative IOD phase (Supplementary Fig. 2a), yet these SST anomalies appear to have played a minor role in this extreme rainfall event. This is because tropical SSTs show limited capacity in modulating the atmospheric circulation anomalies in the higher latitudes of the South Asian monsoon region¹⁶. The regression map of anomalous moisture transport onto the Niño 4 index show that the central Pacific type of La Niña drives westward moisture fluxes cross the Bay of Bengal between 10° and 20°N , but this moisture channel weakens markedly as it advances into the northwestern Indian subcontinent (Supplementary Fig. 2b). This is inconsistent with the observed feature in 2022, in which the anomalous westward moisture transport along Himalayan foothills is stronger than that over the lower-latitudes of south Asia (Fig. 2d). Likewise, the westward moisture transport over northwest of India associated with the negative IOD is also invisible (Supplementary Fig. 2c). Obviously, both the Niño 4 and IOD indices present weak correlations with the simultaneous EI and the SPRI during 1979–2022 (Supplementary Table 1). Moreover, anomalies in these tropical Indo-Pacific SST modes manifest moderate amplitudes in August 2022 in comparison with historical years (Supplementary Table 1), which are unable to explain the rarity of this Pakistan extreme rainfall in 2022. These results suggest that tropical SST anomalies alone exert limited impacts on the anomalous easterly flow over the northwest Indian subcontinent as well as the extreme rainfall within southern Pakistan in 2022, implicating the involvement of additional factors.

Besides the remote influences of SST anomalies, the thermal forcing of the TP has long been recognized as a crucial driver for the onset and maintenance of the SASM^{24,35,36}, especially the atmospheric latent heating associated with rainfall anomalies dominates the total diabatic heating around the TP in summer^{37,38}. Concurrent with the excessive rainfall over southern Pakistan, it is also worth noting that extreme rainfall deficiency is

witnessed around the southeastern slope of TP in August 2022 (Fig. 3a). This rainfall decrease is accompanied by locally reduced condensational heating, whose magnitude is comparable with the vigorous condensational heat release above Pakistan (Fig. 3a). The corresponding vertical profile of condensational heating over southeastern slope of TP also shows that the entire troposphere basically exhibits a reduction in the release of latent heat, resulting in deep diabatic cooling from lower to upper troposphere (Fig. 3b).

From the statistical perspective, the southeastern TP rainfall index (called the STPRI), defined as the regional mean rainfall over $89^\circ\text{--}99^\circ\text{E}/24^\circ\text{--}30^\circ\text{N}$ in August (Supplementary Table 1), is well coupled with the simultaneous release of latent heat in situ during 1979–2022 (Fig. 3c). When rainfall and associated condensational heating over the southeastern TP weaken, the resulting negative diabatic heating anomalies facilitate a westward acceleration of the airflow, yielding a pronounced low-tropospheric easterly anomaly along the southern foothills of the Himalayas (Fig. 3c). More water vapor is thus transported into southern Pakistan from Bay of Bengal and Bangladesh, and evident convergence of moisture flux appears within southern Pakistan (Fig. 3d), promoting enhanced rainfall in this region. Consequently, the STPRI manifests significant correlation coefficients of -0.70 and -0.40 with EI and SPRI during the historical period, respectively (Supplementary Table 1).

The aforementioned results have illustrated a close link between the anomalous easterlies over the northwestern Indian subcontinent and the rainfall anomalies over southeastern TP, yet the cause-and-effect relationship between them remains unclear. Here, we argue that the thermal forcing tied to southeastern TP rainfall could directly drive this anomalous easterly flow. To verify this hypothesis, a numerical experiment with prescribed heat forcing is conducted in the LBM (see Methods). In the simulation, an idealized elliptic heating sink is imposed onto the southeastern slope of TP throughout the integration period (Supplementary Fig. 3a), with its vertical profile prescribed in accordance with the observations (Fig. 3b, Supplementary Fig. 3b). This anomalous heating cools the surrounding air, causing it to contract, become denser, and sink, which raises near-surface pressure in adjacent regions (Supplementary Fig. 3a). Meanwhile, this anomalous near-surface high is accompanied by a lower-tropospheric anticyclone northwest to the heat forcing, thus enhancing the anomalous easterly flow along the Himalayas (Supplementary Fig. 3a), which resembles the Matsuno–Gill response pattern^{39,40}. The simulated circulation anomalies closely match the observed patterns in August 2022 (Fig. 2c), confirming the important role of thermal forcing around TP in this event. The above results are also supported by previous studies^{1,41}, which identified TP heating as a driver of the zonal moisture transport along the Himalayas and monsoon rainfall variability in Pakistan based on the observations during 1980–2014.

Moreover, the STPRI is basically independent of tropical SST forcing, which shows a weak correlation coefficient of -0.17 (-0.10) with the Niño 4 (IOD) index. In August 2022, the STPRI falls to its lowest value since 1979, coinciding with the simultaneous record-breaking EI and SPRI (Supplementary Table 1). These results demonstrate that the anomalous latent-heat linked to rainfall anomalies near the southeastern slope of the TP could directly drive anomalous easterlies over the northwestern Indian subcontinent and enhance precipitation within southern Pakistan, via a pathway that is independent of both ENSO and IOD. This raises the next question: what governs precipitation over the southeastern TP itself? Beyond tropical SSTs, could mid- and high-latitude processes play a role?

Remote modulation of European blocking on rainfall anomalies over the southeastern slope of the TP and Southern Pakistan

From the perspective of the large-scale circulation anomalies across middle and high latitudes of Eurasia, a strong blocking high is observed in the upper troposphere over northeastern Europe, accompanied downstream by an anomalous low extending from Central Asia to Northeast Asia region and an anomalous high over subtropical East Asia (Fig. 4a). This pattern constitutes a stationary Rossby wave train, with apparent wave activity fluxes originated near the European blocking high and propagating downstream (Fig. 4a). The Rossby-wave energy disperses along two pathways, of which

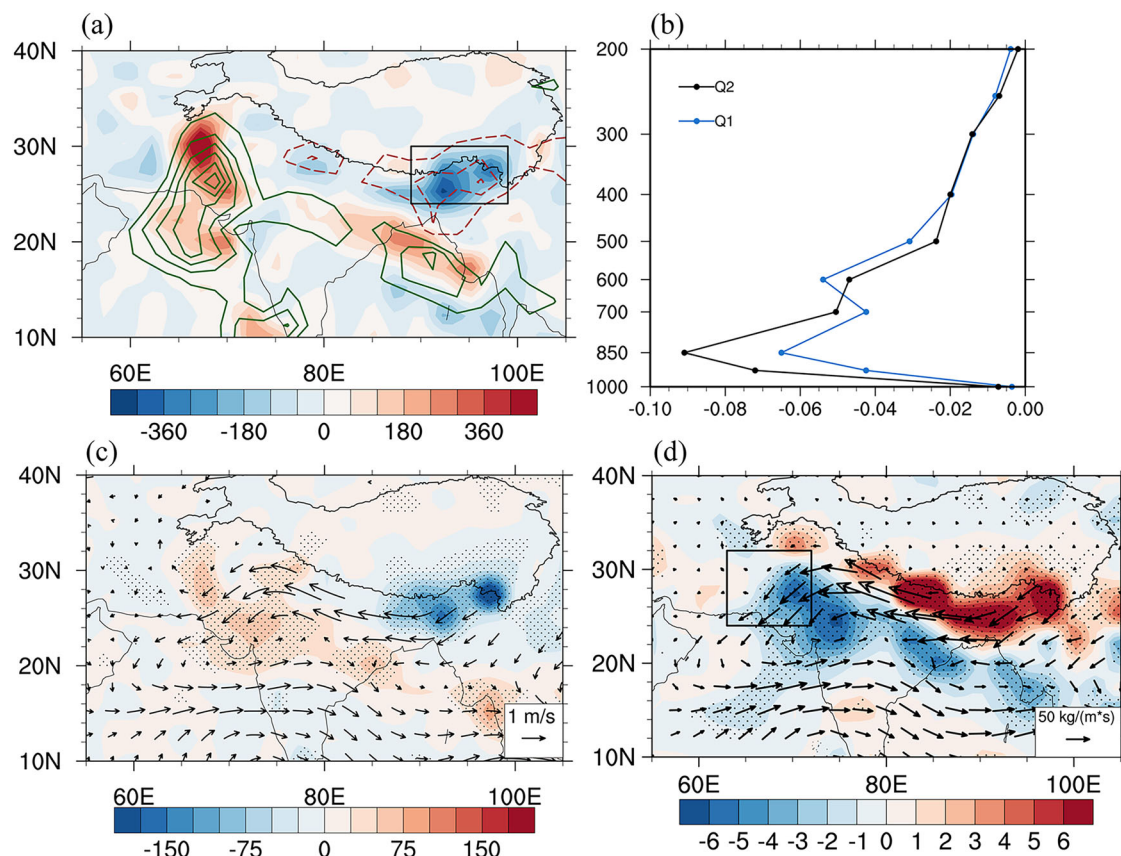


Fig. 3 | The precipitation, diabatic heating and associated anomalous atmospheric circulations in August. **a** The anomalies of both apparent moisture sink (Q_2 ; see Methods) vertically integrated from surface to 300 hPa ($\langle Q_2 \rangle$; shading; $W m^{-2}$) and precipitation ($mm day^{-1}$; contour; interval: 2; negative values are dashed) in 2022. **b** Vertical profiles of apparent heat source (Q_1 ; see Methods) ($W kg^{-1}$; blue) and Q_2 ($W kg^{-1}$; black) averaged over the southeastern TP as denoted by the box in

a, c The regressions of $\langle Q_2 \rangle$ ($W m^{-2}$; shading) and horizontal wind at 850 hPa ($m s^{-1}$; vector) against the standardized STPRI (multiplied by -1) during 1979–2022, in which black dots denote significance at $p = 0.05$ level. **d** Same as in (c), but for the column-integrated moisture flux ($kg m^{-1} s^{-1}$; vector) and its divergence ($\times 10^{-5} kg m^{-2} s^{-1}$; shading).

the stronger one propagates eastward across the Caspian Sea and Lake Baikal toward the East Asia (Fig. 4a). This reinforces the anomalous upper-tropospheric high and attendant anticyclone anchored over subtropical East Asia, since the Rossby-wave activity exerts great effects on the formation and maintenance of midlatitudes anomalous highs⁴².

Along the southern flank of the anomalous anticyclone over subtropical East Asia, upper-tropospheric easterly anomalies dominate the southeastern slope of TP, while zonal wind anomalies over southern Pakistan remain relatively weak (Fig. 4a). Notably, the mid- and upper-tropospheric zonal flow across the TP is crucial for driving local vertical motion in summer, owing to the unique atmospheric thermal structure near the TP^{43–45}. In climatology, a tropospheric warm center with high potential temperature is entrenched over the southwestern TP (Supplementary Fig. 4a), establishing a strong longitudinal potential temperature gradient and an upward inclined isentropic surface from southeastern TP toward middle and lower Yangtze River basin, especially in the mid-upper troposphere (Supplementary Fig. 4b). Since air parcels adiabatically move along the isentropic surfaces⁴⁶, zonal wind anomalies over the southern TP tend to exhibit significant negative correlations with local p-vertical velocity (Supplementary Fig. 4b). Consequently, the pronounced easterly anomalies above the southeastern slope of the TP observed in August 2022 could induce intense descent in situ (Fig. 4b), suppressing the convection and reducing precipitation there (Fig. 3a).

Furthermore, the regressed pattern of upper-tropospheric circulations against the European blocking index (call the EBI; defined in Supplementary Table 1) during 1979–2022 also shows an apparent Rossby wave train across north Europe to subtropical Asia (Fig. 4c), highly consistent with the

observed pattern in August 2022 (Fig. 4a). The anomalous easterly flow at the south flank of the enhanced subtropical East Asian anticyclone slides along the isentropic surface favouring significant descent and reduced rainfall over the southeastern TP (Figs. 4d, 5a). With the bridge role of southeastern TP rainfall and associated condensational heating (Fig. 5a), the European blocking could remotely modulate the anomalous lower-tropospheric easterlies over the northwestern Indian subcontinent, facilitate the moisture transport and convergence over the southern Pakistan (Fig. 5b), and thus enhance the precipitation there (Fig. 5a). Further calculations reveal that the EBI is tightly linked to the STPRI, EI, and SPRI, with significant correlation coefficients during 1979–2022 of -0.57 , 0.45 and 0.38 , respectively (Fig. 5c; Supplementary Table 1). When the influence of southeastern TP rainfall is excluded, the enhanced European blocking high no longer effectively induces anomalous easterly moisture transport over the northwestern Indian subcontinent (Fig. 5d). The partial correlation coefficient between the EBI and SPRI with the variability of STPRI removed becomes statistically insignificant ($r = 0.18$), underscoring the indispensable intermediate role of the southeastern TP condensational heating.

A numerical experiment with the LBM further verifies the downstream influence of the European blocking high. In this experiment, a negative vorticity source is imposed over northeastern Europe ($20^{\circ}E$ – $55^{\circ}E$, $52^{\circ}N$ – $72^{\circ}N$) throughout the integration, to mimic the observed European high anomaly in August 2022. As shown in Supplementary Fig. 5a, the negative vorticity forcing increases geopotential height and induces an anomalous anticyclone in situ. Meanwhile, this blocking high anomaly further triggers a Rossby wave train that propagates towards East Asia and intensifies the subtropical East Asian anticyclone (Supplementary Fig. 5a),

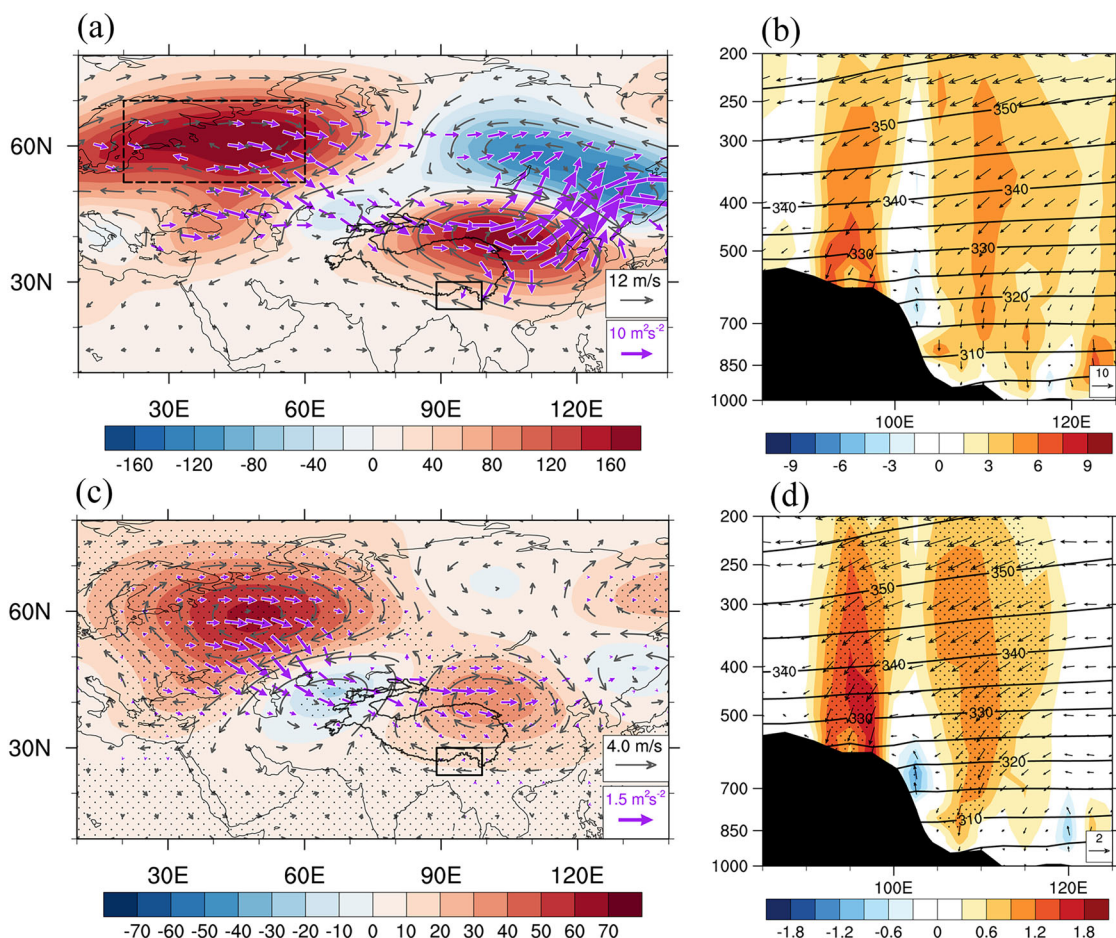


Fig. 4 | The atmospheric teleconnection pattern across Eurasia and vertical motion above the southeastern TP in August. **a** The anomalies of geopotential height (gpm; shading) and horizontal wind (m s^{-1} ; grey vector), and the T-N wave activity flux at 200 hPa ($\text{m}^2 \text{s}^{-2}$; purple vector; only the values exceeding 4 are shown) in 2022, in which the dashed box outlines the region for defining European blocking index (EBI). **b** The pressure-longitude cross section of zonal-vertical circulation (u :

m s^{-1} ; ω : $\times 0.01 \text{ Pa s}^{-1}$; vector) and vertical velocity ($\times 0.01 \text{ Pa s}^{-1}$; shading) averaged over 24° – 31°N in 2022 with the climatological mean potential temperature (K) superposed by contour, in which the black shaded area is for topography along 30°N . **c, d** are same as in **(a, b)**, respectively, but for the regressions against the standardized EBI during 1979–2022, in which black dots denote significance at $p = 0.05$ level.

basically reproducing the observed upper-tropospheric teleconnection pattern of August 2022 (Fig. 4a). However, the lower-tropospheric response exhibits a near-surface low pressure around the TP (Supplementary Fig. 5b), which is distinct from the near-surface high pressure in observation (Fig. 2c). This discrepancy likely arises because the dry version of the LBM neglects the release of condensational heating and its feedback on the atmospheric circulation. To address this issue, an additional TP thermal heating forcing is introduced into the European blocking experiment. This combined-forcing experiment not only simulates the observed upper-level wave train crossing Eurasia (Supplementary Fig. 5c), but also reproduces the near-surface high anomaly and a lower-tropospheric anticyclone extending from TP to northwestern India, thus enhancing the anomalous easterly flow over the northwestern Indian subcontinent (Supplementary Fig. 5d). These results closely resemble the observations (Figs. 2c and 4a), which further confirms the indispensable bridge role of TP condensational heating for conveying the remote influence of European blocking to the South Asia monsoon region.

The aforementioned results delineate a clear physical pathway linking intensified European blocking, reduced southeastern TP rainfall, and excessive rainfall over southern Pakistan observed in 2022. Moreover, the European blocking high in August 2022 ranks as the strongest since 1979 (Supplementary Table 1), confirming its important role in producing the Pakistan extreme rainfall by regulating anomalous southeastern TP heating and zonal moisture transport over the northwestern Indian subcontinent.

Discussion

In the present study, the local and remote atmospheric drivers responsible for the unprecedented Pakistan rainfall event in August 2022 are investigated using observational data and LBM numerical simulation. The water vapor budget over southern Pakistan shows that the westward moisture transport regulated by the anomalous lower-level easterly flows over the northwestern Indian subcontinent dominates the increase of moisture and precipitation within southern Pakistan. Compared with moderate tropical SST anomalies, the extreme rainfall deficiency around the southeastern TP associated with local anomalous diabatic cooling directly drives the pronounced anomalous easterly flow over the northwestern Indian subcontinent. Further analysis reveals that the southeastern TP rainfall is, in turn, governed by mid- and high-latitude processes. In mid- and high-latitudes, an unprecedented European blocking high triggers Rossby-wave energy dispersing toward East Asia and bolsters the anomalous anticyclone there. The pronounced easterly anomalies at the south flank of the East Asian anticyclone, combined with the unique thermal structure over the TP, induce intense descent and reduce rainfall around the southeastern TP. Consequently, the enhanced European blocking could remotely modulate the Pakistan extreme rainfall. Furthermore, both the statistical linkage during 1979–2022 and LBM simulations mirror the observations in 2022, supporting the above conclusions. Our findings highlight the TP heating as an indispensable bridge that connects the

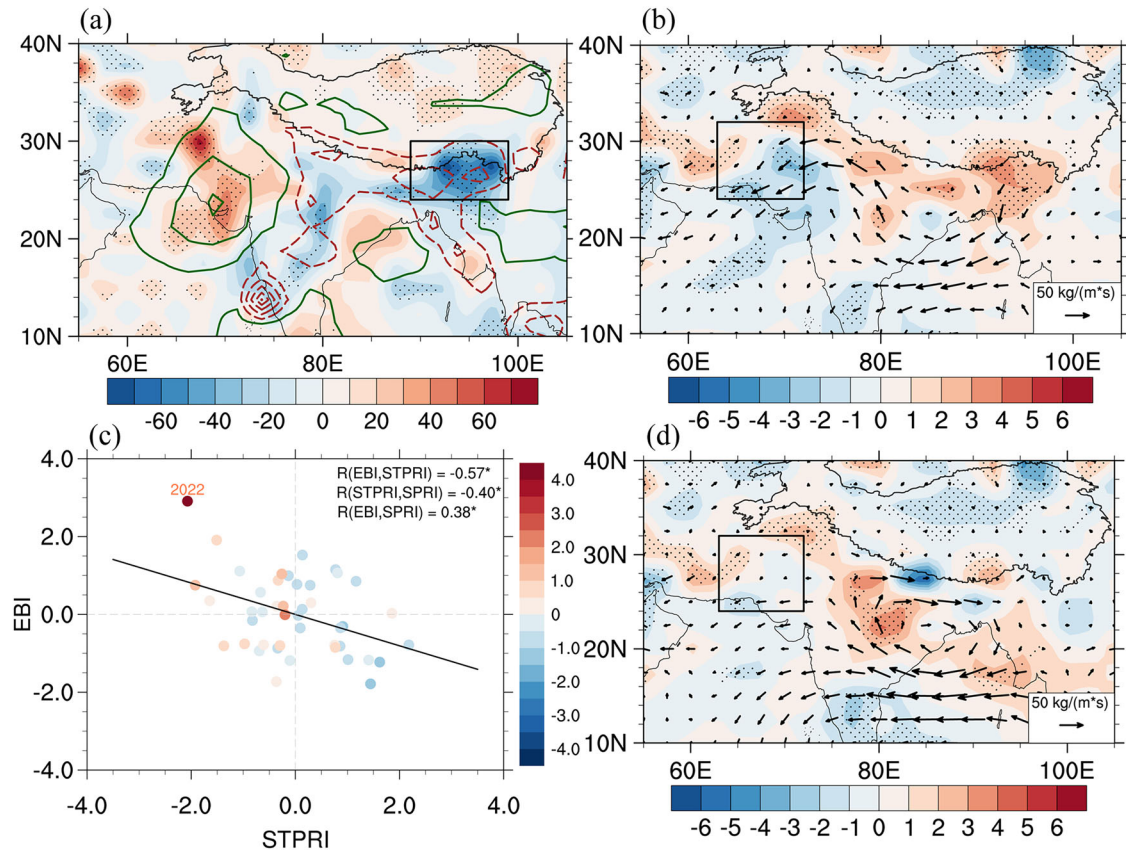


Fig. 5 | The precipitation, diabatic heating and anomalous atmospheric circulations in August associated with enhanced European blocking. **a** The regressions of $\langle Q_2 \rangle$ ($W m^{-2}$; shading), precipitation ($mm day^{-1}$; contour; interval: 0.6) and horizontal wind at 850 hPa ($m s^{-1}$; vector) against the standardized EBI during 1979–2022, in which dots are significant at the $p = 0.05$ level. **b** Same as in (a), but for

the column-integrated moisture flux ($kg m^{-1} s^{-1}$; vector) and its divergence ($\times 10^{-5} kg m^{-2} s^{-1}$; shading). **c** Scatter plot of the standardized STPRI (X-axis), EBI (Y-axis) and SPRI (shading) during 1979–2022, with correlation coefficients between these indices given at the upper right corner. **d** Same as in (b), but for the partial regressions against the standardized EBI with the variability of STPRI eliminated.

European blocking to the southern-Pakistan rainfall extreme by driving the lower-tropospheric westward moisture transport. The conclusions provide an essential supplement for the physical pathway of how the European blocking high influences Pakistan rainfall.

It should be noted that the feedback effect of the local diabatic heating linked to the record-breaking Pakistan rainfall on atmospheric circulations is not considered in this work. Our primary aim is to uncover the causes of the precipitation itself, although condensational heating release that occurs after rainfall onset may further enhance adjacent circulation anomalies and precipitation in situ. Furthermore, the present study mainly focuses on the dynamic modulation of the European blocking high on Pakistan rainfall, but the causes of this intensified European blocking have not been covered in our research yet. This positive height anomaly over Europe persisted for more than one month around August 2022, which may be related to some lower-boundary forcings. For example, the SST anomalies over the North Atlantic Ocean could alter the lower-tropospheric baroclinicity, result in a northward shift of the storm track, and facilitate a positive geopotential height tendency above Europe through eddy vorticity forcing^{47,48}. Arctic SST and sea ice anomalies also contribute to the persistence of Eurasian blocking and equatorward Rossby wave train via local air-ocean-sea ice interaction^{49–51}. Moreover, soil moisture conditions over the European plain could interact with the above atmosphere through latent and sensible heat fluxes, and drought surface conditions produce an enhanced ridging in the mid- and upper-troposphere^{52,53}. The roles of these slow-varying factors warrant further investigations, which will be ultimately beneficial for improving the prediction skill of both TP and Pakistan summer rainfall.

Methods

Data sources

Monthly-mean precipitation on a 2.5° grid for the period 1979–2022 is provided by the Global Precipitation Climatology Project (GPCP), the widely-used global gridded precipitation dataset that synergistically merges satellite-derived estimates with rain gauge observations⁵⁴. The daily maximum surface air temperature on a 0.5° grid for the same period is provided by the National Centers for Environmental Prediction/Climate Prediction Center (NCEP/CPC). All atmospheric circulation variables used in this study are derived from the fifth generation of European Centre for Medium-Range Weather Forecasts (ECMWF) reanalysis (ERA5) with a horizontal resolution of 2.5° ⁵⁵. Monthly-mean sea surface temperature data on a 1° grid comes from the Hadley Centre⁵⁶. Anomalies are calculated as departures from the climatological mean of 1979–2022.

Statistical analysis

Linear correlation and regression are adopted to analyze the relationship between two variables, with their statistical significance tested by the two-tailed Student’s t -test.

Atmospheric apparent heat source/moisture sink

The atmospheric apparent heat source (Q_1) and apparent moisture sink (Q_2)⁵⁷ are estimated from the following Eqs. (1) and (2), respectively:

$$Q_1 = C_p \left(\frac{\partial T}{\partial t} + \vec{V} \cdot \nabla_p T + \left(\frac{p}{p_s} \right)^k \omega \frac{\partial \theta}{\partial p} \right) \quad (1)$$

$$Q_2 = -L \left(\frac{\partial q}{\partial t} + \vec{V} \cdot \nabla_p q + \omega \frac{\partial q}{\partial p} \right) \quad (2)$$

where T , q , \vec{V} , p , ω and θ indicate air temperature, specific humidity, horizontal wind, pressure, vertical velocity and potential temperature, respectively; ∇_p refers to the isobaric gradient operator; $p_s = 1000 \text{ hPa}$ is the surface pressure; $k = \frac{R}{C_p}$, $R = 287 \text{ J kg}^{-1} \text{ K}^{-1}$ and $C_p = 1004 \text{ J kg}^{-1} \text{ K}^{-1}$ are the gas constant and specific heat of dry air at constant pressure, respectively; $L = 2.5 \times 10^6 \text{ J kg}^{-1}$ is the latent heat of condensation.

Wave activity flux

To detect the characteristics of Rossby wave propagation, the two-dimensional T-N wave activity flux based on the quasi-geostrophic framework⁵⁸ is utilized here:

$$\begin{aligned} W = & \frac{p \cos \varphi}{2|U|} \left(\frac{U}{a^2 \cos^2 \varphi} \left[\left(\frac{\partial \psi'}{\partial \lambda} \right)^2 - \psi' \frac{\partial^2 \psi'}{\partial \lambda^2} \right] \right. \\ & + \frac{V}{a^2 \cos \varphi} \left[\frac{\partial \psi'}{\partial \lambda} \frac{\partial \psi'}{\partial \varphi} - \psi' \frac{\partial^2 \psi'}{\partial \lambda \partial \varphi} \right] \frac{U}{a^2 \cos \varphi} \left[\frac{\partial \psi'}{\partial \lambda} \frac{\partial \psi'}{\partial \varphi} - \psi' \frac{\partial^2 \psi'}{\partial \lambda \partial \varphi} \right] \\ & \left. + \frac{V}{a^2} \left[\left(\frac{\partial \psi'}{\partial \varphi} \right)^2 - \psi' \frac{\partial^2 \psi'}{\partial \varphi^2} \right] \right) \quad (3) \end{aligned}$$

where $\psi' = \frac{\phi'}{f}$ denotes the perturbation of geostrophic streamfunction, here ϕ' and f refer to perturbation of geopotential and Coriolis parameter, respectively. Moreover, a is the earth's radius, p is pressure/1000 hPa, and (λ, φ) are longitude and latitude, respectively. $U = (U, V)$ represents the basic flow.

Numerical experiments

The dry version of the linear baroclinic model (LBM) is utilized here to verify the atmospheric responses to prescribed heat forcing and vorticity forcing, based on the observed August mean basic state. The LBM could give a response to prescribed external forcing (including vorticity, divergence, temperature, and surface pressure perturbations) via adiabatic processes⁵⁹. This model simplifies the dynamic framework of the atmospheric general circulation model (AGCM) and excludes complex nonlinear processes and various feedback mechanisms in the atmosphere, making its results much easier to be interpreted in comparison with those in AGCM^{59,60}. In this study, the model with a horizontal resolution of T42 (roughly $2.8^\circ \times 2.8^\circ$) and vertical 20 levels of sigma (σ) coordinate system is adopted, using a time integration method continued up to 30 days. Given that the atmospheric responses generally approach the quasi-steady state around 30 days, the last 5-day average of the 30-day integration could be considered as an equilibrated response⁶¹.

Data availability

Atmospheric reanalysis datasets used in this study are openly available from the ERA5 at <https://cds.climate.copernicus.eu/datasets?q=ERA5&limit=30>; precipitation dataset is provided by GPCP at <https://psl.noaa.gov/data/gridded/data.gpcp.html>; The daily maximum surface air temperature is provided by the NCEP/CPC at <https://www.psl.noaa.gov/data/gridded/data.cpc.globaltemp.html>; SST dataset is provided by Hadley Centre at <https://www.metoffice.gov.uk/hadobs/hadisst/>.

Received: 25 November 2025; Accepted: 13 February 2026;

Published online: 02 March 2026

References

1. Wang, Z. et al. Tibetan Plateau heating as a driver of monsoon rainfall variability in Pakistan. *Clim. Dyn.* **52**, 6121–6130 (2019).

2. Lu, R., Hina, S. & Hong, X. Upper- and Lower-tropospheric Circulation Anomalies Associated with Interannual Variation of Pakistan Rainfall during Summer. *dqkxjz* **37**, 1179–1190 (2020).
3. Ahmad, I. et al. Probability analysis of monthly rainfall on seasonal monsoon in Pakistan. *Int. J. Climatol.* **34**, 827–834 (2014).
4. Ali, S. et al. Spatio-Temporal Variability of Summer Monsoon Onset over Pakistan. *Asia-Pac. J. Atmos. Sci.* **56**, 147–172 (2020).
5. Malik, I., Chuphal, D. S., Vegad, U. & Mishra, V. Was the extreme rainfall that caused the August 2022 flood in Pakistan predictable? *Environ. Res.: Clim.* **2**, 041005 (2023).
6. Luo, Y. et al. The impact of tropical sea surface temperature on extreme precipitation in Pakistan during the summer of 2022. *Environ. Res. Lett.* **19**, 044012 (2024).
7. Mallapaty, S. Why are Pakistan's floods so extreme this year? *Nature* <https://doi.org/10.1038/d41586-022-02813-6> (2022).
8. Nanditha, J. S. et al. The Pakistan Flood of August 2022 Causes and Implications. *Earth's Future* **11**, e2022EF003230 (2023).
9. Ashok, K., Guan, Z. & Yamagata, T. Impact of the Indian Ocean dipole on the relationship between the Indian monsoon rainfall and ENSO. *Geophys. Res. Lett.* **28**, 4499–4502 (2001).
10. Krishnaswamy, J. et al. Non-stationary and non-linear influence of ENSO and Indian Ocean Dipole on the variability of Indian monsoon rainfall and extreme rain events. *Clim. Dyn.* **45**, 175–184 (2015).
11. Hrudya, P. H., Varikoden, H. & Vishnu, R. A review on the Indian summer monsoon rainfall, variability and its association with ENSO and IOD. *Meteorol. Atmos. Phys.* **133**, 1–14 (2021).
12. Zhang, S., Qu, X., Huang, G. & Hu, P. Asymmetric response of South Asian summer monsoon rainfall in a carbon dioxide removal scenario. *npj Clim. Atmos. Sci.* **6**, 1–11 (2023).
13. Rasmusson, E. M. & Carpenter, T. H. The Relationship Between Eastern Equatorial Pacific Sea Surface Temperatures and Rainfall over India and Sri Lanka. *Monthly Weather Rev.* **111**, 517–528 (1983).
14. Aneesh, S. & Sijikumar, S. Changes in the La Niña teleconnection to the Indian summer monsoon during recent period. *J. Atmos. Sol.-Terrestrial Phys.* **167**, 74–79 (2018).
15. Hong, C.-C. et al. Causes of 2022 Pakistan flooding and its linkage with China and Europe heatwaves. *npj Clim. Atmos. Sci.* **6**, 1–10 (2023).
16. Tang, S. et al. Linkages of unprecedented 2022 Yangtze River Valley heatwaves to Pakistan flood and triple-dip La Niña. *npj. Clim. Atmos. Sci.* **6**, 1–8 (2023).
17. Hussain, M. S., Kim, S. & Lee, S. On the relationship between Indian Ocean Dipole events and the precipitation of Pakistan. *Theor. Appl. Climatol.* **130**, 673–685 (2017).
18. Lau, W. K. M. & Kim, K.-M. The 2010 Pakistan Flood and Russian Heat Wave: Teleconnection of Hydrometeorological Extremes. <https://doi.org/10.1175/JHM-D-11-016.1> (2012).
19. Hong, C.-C., Hsu, H.-H., Lin, N.-H. & Chiu, H. Roles of European blocking and tropical-extratropical interaction in the 2010 Pakistan flooding. *Geophys. Res. Lett.* **38**, L13806 (2011).
20. Galareau, T. J. Jr., Hamill, T., Dole, R. & Perlwitz, J. A Multiscale Analysis of the Extreme Weather Events over Western Russia and Northern Pakistan during July 2010. *Monthly Weather Rev.* **140**, 1639–1664 (2012).
21. Di Capua, G. et al. Drivers behind the summer 2010 wave train leading to Russian heatwave and Pakistan flooding. *npj Clim. Atmos. Sci.* **4**, 1–14 (2021).
22. Yamada, T. J., Takeuchi, D., Farukh, M. A. & Kitano, Y. Climatological Characteristics of Heavy Rainfall in Northern Pakistan and Atmospheric Blocking over Western Russia. *J. Clim.* **29**, 7743–7754 (2016).
23. Hu, X. et al. Comparative Analysis of Characteristics and Physical Mechanisms for Typical Summer Extreme Precipitation in Pakistan. *Environ. Res. Commun.* <https://doi.org/10.1088/2515-7620/ad3c18> (2024).

24. Wu, G. et al. The Influence of Mechanical and Thermal Forcing by the Tibetan Plateau on Asian Climate. *J. Hydrometeorol.* **8**, 770–789 (2007).
25. Wu, G. et al. Tibetan Plateau climate dynamics: recent research progress and outlook. *Natl. Sci. Rev.* **2**, 100–116 (2015).
26. Zhao, P., Zhou, X., Chen, J., Liu, G. & Nan, S. Global climate effects of summer Tibetan Plateau. *Sci. Bull.* **64**, 1–3 (2019).
27. Liu, Y. et al. Land–atmosphere–ocean coupling associated with the Tibetan Plateau and its climate impacts. *Natl. Sci. Rev.* **7**, 534–552 (2020).
28. Liu, Y. et al. The Tibetan Plateau bridge: Influence of remote teleconnections from extratropical and tropical forcings on climate anomalies. *Atmos. Ocean. Sci. Lett.* **17**, 100396 (2024).
29. Yanai, M., Li, C. & Song, Z. Seasonal Heating of the Tibetan Plateau and Its Effects on the Evolution of the Asian Summer Monsoon. *J. Meteorol. Soc. JPN* **70**, 319–351 (1992).
30. Zhao, P. & Chen, L. Interannual variability of atmospheric heat source/sink over the Qinghai–Xizang (Tibetan) Plateau and its relation to circulation. *Adv. Atmos. Sci.* **18**, 106–116 (2001).
31. Duan, A. & Wu, G. Role of the Tibetan Plateau thermal forcing in the summer climate patterns over subtropical Asia. *Clim. Dyn.* **24**, 793–807 (2005).
32. He, B., Liu, Y., Wu, G., Wang, Z. & Bao, Q. The role of air–sea interactions in regulating the thermal effect of the Tibetan–Iranian Plateau on the Asian summer monsoon. *Clim. Dyn.* **52**, 4227–4245 (2019).
33. Cui, Y., Duan, A., Liu, Y. & Wu, G. Interannual variability of the spring atmospheric heat source over the Tibetan Plateau forced by the North Atlantic SSTA. *Clim. Dyn.* **45**, 1617–1634 (2015).
34. Wang, Z., Yang, S., Lau, N.-C. & Duan, A. Teleconnection between Summer NAO and East China Rainfall Variations: A Bridge Effect of the Tibetan Plateau. *J. Clim.* **31**, 6433–6444 (2018).
35. He, H., McGinnis, J. W., Song, Z. & Yanai, M. Onset of the Asian Summer Monsoon in 1979 and the Effect of the Tibetan Plateau. *Monthly Weather Rev.* **115**, 1966 (1987).
36. Jiang, X. & Ting, M. A Dipole Pattern of Summertime Rainfall across the Indian Subcontinent and the Tibetan Plateau. <https://doi.org/10.1175/JCLI-D-16-0914.1> (2017).
37. Hu, J. & Duan, A. Relative contributions of the Tibetan Plateau thermal forcing and the Indian Ocean Sea surface temperature basin mode to the interannual variability of the East Asian summer monsoon. *Clim. Dyn.* **45**, 2697–2711 (2015).
38. Jiang, X., Li, Y., Yang, S., Yang, K. & Chen, J. Interannual Variation of Summer Atmospheric Heat Source over the Tibetan Plateau and the Role of Convection around the Western Maritime Continent. <https://doi.org/10.1175/JCLI-D-15-0181.1> (2016).
39. Matsuno, T. Quasi-Geostrophic Motions in the Equatorial Area. *J. Meteorological Soc. Jpn. Ser. II* **44**, 25–43 (1966).
40. Gill, A. E. Some simple solutions for heat-induced tropical circulation. *Q. J. R. Meteorological Soc.* **106**, 447–462 (1980).
41. Wang, Z., Duan, A., Li, M. & He, B. Influences of thermal forcing over the slope/platform of the Tibetan Plateau on Asian summer monsoon: Numerical studies with the WRF model. *Chin. J. Geophysics* **59**, 3175–3187 (2016).
42. Enomoto, T., Endo, H., Harada, Y. & Ohfuchi, W. Relationship between High-Impact Weather Events in Japan and Propagation of Rossby Waves along the Asian Jet in July 2004. *J. Meteorological Soc. Jpn. Ser. II* **87**, 139–156 (2009).
43. He, C., Zhou, T., Zhang, L., Chen, X. & Zhang, W. Extremely hot East Asia and flooding western South Asia in the summer of 2022 tied to reversed flow over Tibetan Plateau. *Clim. Dyn.* **61**, 2103–2119 (2023).
44. He, C. et al. Contrasting East Asian climate extremes in 2020 and 2022 tied to zonal flow. *Environ. Res. Lett.* **19**, 104019 (2024).
45. Wang, Z., Luo, H. & Yang, S. Different mechanisms for the extremely hot central-eastern China in July–August 2022 from a Eurasian large-scale circulation perspective. *Environ. Res. Lett.* **18**, 024023 (2023).
46. Holton, J. R. An Introduction to Dynamic Meteorology. In <https://doi.org/10.1119/1.1987371> (2004).
47. Sun, J. Record-breaking SST over mid-North Atlantic and extreme high temperature over the Jianghuai–Jiangnan region of China in 2013. *Chin. Sci. Bull.* **59**, 3465–3470 (2014).
48. Yin, Z., Yang, S. & Wei, W. Prevalent atmospheric and oceanic signals of the unprecedented heatwaves over the Yangtze River Valley in July–August 2022. *Atmos. Res.* **295**, 107018 (2023).
49. Ruggieri, P., Buizza, R. & Visconti, G. On the link between Barents–Kara sea ice variability and European blocking. *J. Geophys. Res.: Atmospheres* **121**, 5664–5679 (2016).
50. Chen, X., Dai, A., Wen, Z. & Song, Y. Contributions of Arctic Sea-Ice Loss and East Siberian Atmospheric Blocking to 2020 Record-Breaking Meiyu-Baiu Rainfall. *Geophys. Res. Lett.* **48**, e2021GL092748 (2021).
51. Zhang, P., Wang, B., Wu, Z., Jin, R. & Cao, C. Intensified gradient La Niña and extra-tropical thermal patterns drive the 2022 East and South Asian “Seesaw” extremes. *npj Clim. Atmos. Sci.* **7**, 1–9 (2024).
52. Fischer, E. M., Seneviratne, S. I., Vidale, P. L., Lüthi, D. & Schär, C. Soil Moisture–Atmosphere Interactions during the 2003 European Summer Heat Wave. *J. Clim.* **20**, 5081–5099 (2007).
53. Zhang, T. et al. Synergistic contribution of soil moisture and sea surface temperature to summer Tibetan Plateau temperature. *Atmos. Res.* **314**, 107811 (2025).
54. Adler, R. F. et al. The Global Precipitation Climatology Project (GPCP) Monthly Analysis (New Version 2.3) and a Review of 2017 Global Precipitation. *Atmosphere* **9**, 138 (2018).
55. Hersbach, H. et al. The ERA5 global reanalysis. *Q. J. Roy. Meteor. Soc.* **146**, 1999–2049 (2020).
56. Rayner, N. A. et al. Global analyses of sea surface temperature, sea ice, and night marine air temperature since the late nineteenth century. *J. Geophys. Res. Atmos.* **108**, 4407 (2003).
57. Yanai, M., Esbensen, S. & Chu, J.-H. Determination of Bulk Properties of Tropical Cloud Clusters from Large-Scale Heat and Moisture Budgets. *J. Atmos. Sci.* **30**, 611–627 (1973).
58. Takaya, K. & Nakamura, H. A Formulation of a Phase-Independent Wave-Activity Flux for Stationary and Migratory Quasigeostrophic Eddies on a Zonally Varying Basic Flow. *J. Atmos. Sci.* **58**, 608–627 (2001).
59. Watanabe, M. & Kimoto, M. Atmosphere–ocean thermal coupling in the North Atlantic: A positive feedback. *Q. J. R. Meteorological Soc.* **126**, 3343–3369 (2000).
60. Lu, R. & Lin, Z. Role of Subtropical Precipitation Anomalies in Maintaining the Summertime Meridional Teleconnection over the Western North Pacific and East Asia. *J. Clim.* **22**, 2058–2072 (2009).
61. Zhong, W. & Wu, Z. Subseasonal variations of Eurasian wintertime surface air temperature: two distinct leading modes. *Clim. Dyn.* **59**, 85–108 (2022).

Acknowledgements

This work was jointly supported by the National Key Research and Development Program of China (Grants 2023YFC3007501), the major science and technology project of the Xizang Autonomous Region (XZ202402ZD0006), the National Natural Science Foundation of China (Grants 42075045), and the Youth Innovation Team of China Meteorological Administration “Climate change and its impacts in the Tibetan Plateau” (CMA2023QN16).

Author contributions

J.Y. acquired the datasets, performed the calculations, and drafted the manuscript. X.J. conceived the idea and discussed the results. T.Z. discussed the results and revised the manuscript. C.C. supervised the study

and acquired the funding. H.W. performed the calculations. All authors engaged in the discussion of the results and contributed to the revision.

Competing interests

The authors declare no competing interests.

Additional information

Supplementary information The online version contains supplementary material available at <https://doi.org/10.1038/s41612-026-01358-z>.

Correspondence and requests for materials should be addressed to Xingwen Jiang.

Reprints and permissions information is available at <http://www.nature.com/reprints>

Publisher's note Springer Nature remains neutral with regard to jurisdictional claims in published maps and institutional affiliations.

Open Access This article is licensed under a Creative Commons Attribution-NonCommercial-NoDerivatives 4.0 International License, which permits any non-commercial use, sharing, distribution and reproduction in any medium or format, as long as you give appropriate credit to the original author(s) and the source, provide a link to the Creative Commons licence, and indicate if you modified the licensed material. You do not have permission under this licence to share adapted material derived from this article or parts of it. The images or other third party material in this article are included in the article's Creative Commons licence, unless indicated otherwise in a credit line to the material. If material is not included in the article's Creative Commons licence and your intended use is not permitted by statutory regulation or exceeds the permitted use, you will need to obtain permission directly from the copyright holder. To view a copy of this licence, visit <http://creativecommons.org/licenses/by-nc-nd/4.0/>.

© The Author(s) 2026